Microelectronics Reliability 109 (2020) 113658

Contents lists available at ScienceDirect

Microelectronics Reliability

journal homepage: www.elsevier.com/locate/microrel

Spectral efficiency of lutetium aluminum garnet ($Lu_3Al_5O_{12}$:Ce) with microelectronic optical sensors

C. Michail[a], K. Ninos[b], N. Kalyvas[a], A. Bakas[b], G. Saatsakis[c], G. Fountos[a], I. Sianoudis[b], G. Panayiotakis[c], I. Kandarakis[a], I. Valais[a,*]

[a] Department of Biomedical Engineering, Radiation Physics, Materials Technology and Biomedical Imaging Laboratory, University of West Attica, Ag. Spyridonos, 12210 Athens, Greece
[b] Department of Biomedical Sciences, University of West Attica, Ag. Spyridonos, 12210 Athens, Greece
[c] Department of Medical Physics, Faculty of Medicine, University of Patras, 265 00 Patras, Greece

ARTICLE INFO

Keywords:
Inorganic scintillators
Single crystals
Radiation detectors
$Lu_3Al_5O_{12}$:Ce
$(Lu,Gd)_2SiO_5$:Ce
Lu_2SiO_5:Ce

ABSTRACT

The aim of the present work was to investigate the absolute luminescence efficiency (AE) of a lutetium aluminum $Lu_3Al_5O_{12}$:Ce (LuAG:Ce) garnet, doped with cerium, combined with various microelectronic optical sensors. Two LuAG:Ce samples, with dimensions of 5 × 5 × 10 and 10 × 10 × 10 mm^3 were examined. The light emitted by the crystals, was evaluated by performing measurements of the AE using X-rays from 50 to 130 kV. The spectral compatibility of the LuAG:Ce crystal, with various existing optical detectors, was investigated after emission spectra measurements. Results were compared with previously published data for commercially available lutetium based and cerium doped crystals, such as, $(Lu,Gd)_2SiO_5$:Ce and Lu_2SiO_5:Ce, frequently used in medical imaging applications. Absolute efficiency was found maximum at 130 kVp for the 5 × 5 × 10 mm^3 LuAG:Ce crystal (31.86 efficiency units-E.U). AE of the 10 × 10 × 10 mm^3 LuAG:Ce crystal was found higher than both LGSO:Ce and LSO:Ce crystals (of equal dimensions). The emission spectrum of LuAG:Ce is excellent matched with the spectral sensitivities of photocathodes, charge coupled devices (CCD), non-passivated amorphous hydrogenated silicon photodiodes (a-Si:H) and complementary metal-oxide semiconductors (CMOS) microelectronic devices employed in radiation detection. Considering the higher luminescence efficiency values than currently used crystals and the spectral compatibility with the various photodetectors, LuAG:Ce single crystal could be considered for use in imaging detectors, such as, PET/CT scanners.

1. Introduction

Scintillators, coupled with microelectronic optical detectors, such as complementary metal-oxide semiconductor (CMOS) and charge-coupled devices (CCD), photocathodes and photomultipliers, are used as radiation converters in various imaging applications [1,2]. These materials, even in nanoscale, are widely used in applications such as high energy physics, homeland security and in various disciplines of medical imaging [3–16].

Research and development of today's state-of-the-art microelectronic imaging systems require scintillators with properties satisfying the requirements of numerous disciplines [1,17–19]. In the case of time of flight positron emission tomography (PET) scanners, there is the need for dense scintillators with decay time of a few nano seconds and high light yield [20]. Slow components in the scintillation decay of these scintillators can degrade the quality of PET images [7]. Similarly, in computed tomography (CT), the use of scintillators with afterglow can result in image blurring [7].

Other demanding X-ray imaging applications, with fast framing rates and short exposure times, investigating dynamic processes (fluid dynamics, mechanical motions, blood flow, etc.), require also efficient scintillators [19].

Various scintillating crystals has been used up to now, such as, bismuth germinate oxide (BGO), yttrium orthoaluminate perovskite ($YAlO_3$:Ce or YAP), lutetium orthoaluminate perovskite $LuAlO_3$:Ce or LuAP:Ce, lutetium yttrium orthoaluminate perovskite ($(LuY)AlO_3$:Ce or LuYAP:Ce), lutetium oxyorthosilicate (Lu_2SiO_5:Ce or LSO), gadolinium oxyorthosilicate (Gd_2SiO_5:Ce or GSO) and various others [21–23].

Besides these, $Lu_3Al_5O_{12}$ scintillators, activated by cerium (Ce), praseodymium (Pr) or scandium (Sc) (LuAG:Ce, LuAG:Pr, and LuAG:Sc) has been used for radiation monitoring and CT applications [18,24]. $Lu_3Al_5O_{12}$:Ce is one of the most promising materials of the last fifteen

* Corresponding author.
E-mail address: valais@uniwa.gr (I. Valais).

https://doi.org/10.1016/j.microrel.2020.113658
Received 17 July 2019; Received in revised form 19 February 2020; Accepted 7 April 2020
Available online 25 April 2020

years and has been thoroughly studied, in single crystal form, from various research groups [3,25–32]. It has relatively high density of 6.73 g/cm^3 (significantly higher than materials such as YAG), effective atomic number Z = 62.9, and light yield values from 16,700 to 27,000 photons/MeV have been reported [5,30,33–35]. Ce^{3+} doped LuAG has intense and prompt emission with a maximum at around 535 nm, due to the 5d–4f radiative transitions of Ce^{3+} ions [36,37]. LuAG:Ce has relatively fast scintillation response (around 69 ns), slower than that of LSO:Ce (~40 ns) which has been already successfully applied in time of flight PET applications [38]. The energy resolution (ER) has been previously reported 6.5% at 662 keV [38] and the refractive index with a value of 1.84 [39]. The thermal conductivity of LuAG:Ce has a value of 9.6 W m^{-1} K^{-1}, the specific heat is 0.411 J g^{-1} K^{-1} and the thermal expansion coefficient is 8.8 × 10^{-6} (C^{-1}) [19,40,41].

LuAG:Ce, besides in single crystal form, has been alternatively fabricated in order to optimize its scintillator properties, such as the light yield and to minimize manufacturing costs [42–46]. For example, LuAG:Ce, has been fabricated using the liquid phase epitaxy method, for optoelectronic applications [46]. Also, has been used as phoswich (phosphor sandwich) in order to detect different components of ionizing radiation. In these experiments the luminescent properties of composite scintillators, based on single crystalline films of LuAG:Ce has been investigated [24,39,47,48]. LuAG:Ce has been also studied for applications in light emitting diodes (LEDs) and electromagnetic calorimetry [5,34,49,50].

The purpose of the present study was to examine the spectral matching efficiency of LuAG:Ce crystal samples, for applications in medical imaging detectors, using X-ray radiation. The spectral matching of the examined samples emitted spectra with various microelectronic optical sensors was determined, by performing spectral and efficiency measurements. The efficiency of the examined samples were compared with commercially available mixed oxyorthosilicate lutetium based, cerium doped $(Lu,Gd)_2SiO_5$:Ce (LGSO:Ce) and LSO single crystals.

2. Materials and methods

LuAG:Ce polished single crystals were purchased from Advatech UK Limited with dimensions of 5 × 5 × 10 mm and 10 × 10 × 10 mm. The crystals were irradiated with X-rays from 50 to 130 kVp with a BMI General Medical Merate unit [51]. An additional filtration equal to 20 mm Al was added at the exit of the X-ray tube to account for the attenuation of a human body and in order for the results to be comparable with published data [52].

2.1. Absolute efficiency (AE)

The efficiency of a scintillator to emit light, after ionizing radiation exposure, can be experimentally determined by calculating the absolute luminescence efficiency (n_A), defined as the ratio of the emitted light energy flux $\dot{\Psi}\lambda$ over the radiation exposure rate, $\dot{X}$ that is [13–15,21,52,53]:

$$\eta_A = \dot{\Psi}_\lambda / \dot{X} \quad (1)$$

n_A is expressed in efficiency units (E.U.) μW × m^{-2}/(mR × s^{-1}). The light flux measurements were performed using a light integrating sphere (Oriel 70451 barium sulfate coating) which was coupled to a photomultiplier tube (PMT) (EMI 9798B) with ES-20 photocathode. The spectral sensitivity of the photocathode is shown in Fig. 2a. The PMT was connected to a Cary 401 vibrating reed electrometer. The radiation exposure rate incident at the scintillator surface was measured by means of an RTI Piranha P100B dosimeter.

2.2. Spectral matching factor (α_s) and effective efficiency (η_{eff})

The efficiency of an optical sensor to capture the light emitted from a scintillator, can be determined through the spectral matching factor α_s, which is:

$$\alpha_s = \int \phi_\lambda(\lambda) S_D(\lambda) d\lambda / \int \phi_\lambda(\lambda) d\lambda \quad (2)$$

where $\phi_\lambda(\lambda)$ is the light spectrum emitted by the crystal and $S_D(\lambda)$ is the normalized spectral sensitivity distribution of the sensor [53].

The emitted light was measured by a grating optical spectrometer (Ocean Optics Inc., HR2000). The spectral sensitivities of the optical detectors were obtained from manufacturers' data and published literature [54–58]. The term effective efficiency was initially introduced by Cavouras et al. [59] in order to evaluate the degradation of the absolute luminescence efficiency when coupled to particular optical sensors. The effective efficiency n_{eff} was calculated as the product of n_A with the spectral matching factor, that is [21]:

$$n_{eff} = n_A \alpha_s \quad (3)$$

2.3. Ionizing radiation absorption efficiency

The radiation detection properties of a scintillator can be quantified by the quantum detection efficiency (QDE) and the energy absorption efficiency (EAE) [60,61]. QDE corresponds to the fraction of incident photons interacting within the scintillator mass [62]. EAE is calculated using the energy absorption coefficient depicting the energy locally deposited at the sites of primary photon interactions. It excludes all types of secondary photons originating from the point of initial photon interaction (Compton scattering, K-fluorescence, Bremsstrahlung), thus it is a useful parameter in estimating the efficiency in projection imaging modalities. QDE and EAE were evaluated analytically following previous studies [60,61]. Total attenuation and total energy absorption coefficients of the examined crystals were calculated using tabulated data from tables of X-ray mass attenuation coefficients and mass energy absorption coefficients of lutetium, aluminum and oxygen of the National Institute of Standards and Technology (NIST) of the US Department of commerce [58,62].

3. Results and discussion

Fig. 1 shows the variation of absolute luminescence efficiency of the two LuAG:Ce single crystals. Results are shown for the X-rays from 50 to

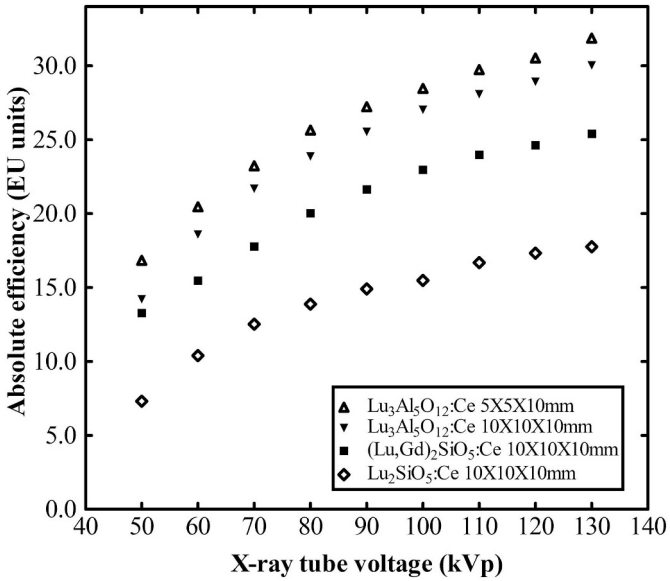

Fig. 1. Absolute luminescence efficiency comparison of the 5 × 5 × 10 and 10 × 10 × 10 mm^3 LuAG:Ce crystals with previously published data for LGSO:Ce and LSO:Ce single crystals.

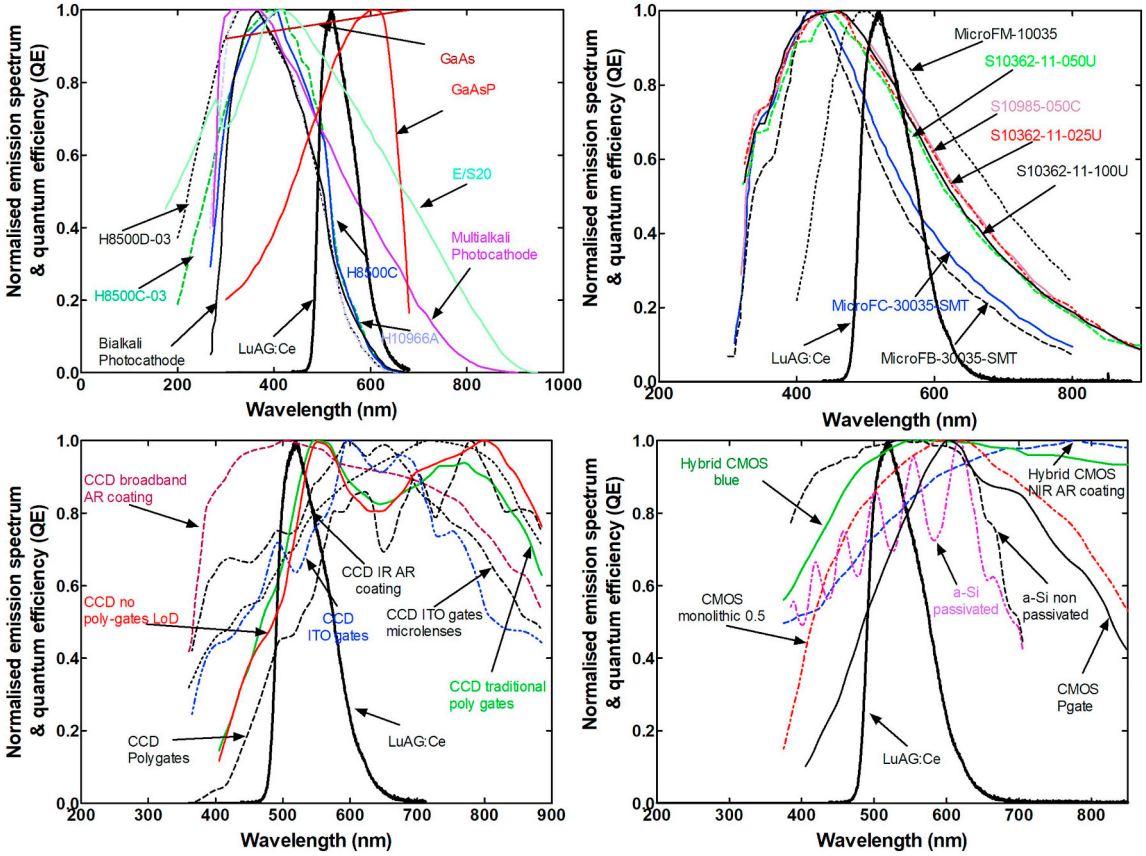

Fig. 2. Normalized emitted light spectrum of the LuAG:Ce crystal and spectral sensitivity of various light detectors.

130 kVp. Fig. 1 also shows a comparison of the emission performance with previously published data, for LGSO:Ce and LSO:Ce crystals of equal dimensions (10 × 10 × 10 mm^3) [21]. AE of all crystals are increasing up to the X-ray tube voltage setting of 130 kVp. Absolute efficiency maximized at 130 kVp for the 5 × 5 × 10 mm^3 crystal with a value of 31.86 E.U. The 10 × 10 × 10 mm^3 LuAG:Ce crystal showed higher absolute luminescence efficiency (30.03 E.U, at 130 kVp) than both LGSO:Ce and LSO:Ce, across the examined energy range [21,62]. The AE value of the 10 × 10 × 10 mm^3 LSO:Ce scintillator sample (standard scintillator in PET scanners), which has been measured under the same conditions, was found equal to 18 E.U. and that of LGSO:Ce was equal to 25.39 E.U. These differences can be attributed to the non-proportionality of this crystal's light yield in this energy range [5,27]. Non-proportionality of the light yield values for LuAG:Ce and LSO:Ce at 16.6 keV, with deviations from unity of about 22% and 45%, respectively has been reported [5,27,63–65].

Fig. 2 shows the emitted optical spectrum of LuAG:Ce crystal, normalized to unity and the normalized sensitivity of various optical photon detectors. The LuAG:Ce spectrum shows a maximum at ~525 nm, lying within the green region of the spectrum, resulting in a mean light photon energy ($\overline{E_\lambda} = hc/\overline{\lambda}$) of 2.37 eV. The emission around 500–550 nm is attributed to the 5d–4f transition of Ce^{3+} ions [33].

Table 1 shows the spectral matching factors values of the LuAG:Ce with optical detectors. Such detectors are various types of photocathodes, position sensitive and silicon photomultipliers (SiPMs), used in indirect nuclear medical imaging detectors. LuAG:Ce exhibits excellent compatibility with a non-passivated amorphous hydrogenated silicon photodiode (a-Si:H) (0.99), employed in photodiodes and thin film transistors of flat panel detectors. Furthermore, shows excellent compatibility when coupled with a hybrid complementary metal-oxide semiconductor (CMOS) (0.98), used in digital radiography and mammography systems. Furthermore, with photocathodes, incorporated in various types of photomultipliers, such as gallium arsenide photocathodes GaAs (0.97). The same value was found for the spectral matching when coupled with microelectronic charge-coupled devices (CCD) having broadband anti-reflection coating (0.97). LuAG:Ce also showed excellent compatibility with a monolithic (0.25 μm) (0.92) and a high resolution RadEye CMOS (0.89), as well as with a CCD having traditional polygates (0.87). It was found with good compatibility with Hamamatsu MPPC silicon photomultipliers (0.79 for S10985, 0.79 for S10362-11-050U and 0.78 for S10362-11-100U) and with Sensl's silicon photomultiplier MicroFM-10,035 (0.79). The rest of the Sensl's silicon PMTs show moderate values, for example 0.59 for the MicroFC-30035. It was found incompatible with Hamamatsu flat panel position sensitive photomultipliers, such as the H8500C-03 (0.38).

Fig. 3 shows the effective luminescence efficiency of the LuAG:Ce crystal with various optical detectors. The best effective luminescence efficiency was found for the non-passivated amorphous hydrogenated silicon photodiode (a-Si:H) (matching factor 0.99) and the worst with the flat panel PS-PMT H10966A (0.29) which is shifted to higher wavelengths. Taking into account these data and the higher luminescence efficiency values of LuAG:Ce compared with other widely used lutetium based and cerium doped crystals could be efficiently coupled to various types of optical photon detectors and especially to silicon photomultipliers in combined PET/CT detectors.

Table 2 shows energy absorption efficiency values of the 10 mm thick LuAG:Ce crystal and comparison with $(Lu50\%,Gd50\%)_2SiO_5$:Ce and LSO. Values are shown in the range 50 to 130 kV. EAE requires calculations of the mass energy absorption and attenuation coefficients for the examined single crystals. The values of the coefficients were calculated from tabulated data. Energy absorption efficiency values, at 40 kVp, for all three crystals are almost equal, LGSO (0.877), following LSO with 0.875 and LuAG with 0.872. The difference from unity is explained considering the fact that EAE does not include the effect of

Table 1
Spectral matching factors.

Optical detectors	$Lu_3Al_5O_{12}$:Ce	Optical detectors	$Lu_3Al_5O_{12}$:Ce
CCD broadband AR coating	0.97	GaAsP phosphor photocathode	0.84
CCD infrared (IR) anti-reflection (AR) coating	0.77	Extended photocathode (E-S20)	0.78
CMOS hybrid with blue anti-reflection (AR) coating	0.81	Si PM MicroFC-30035-SMT	0.59
Hybrid CMOS blue	0.98	Si PM MicroFB-30035-SMT	0.52
CMOS (monolithic 0.25 μm)	0.92	Si PM MicroFM-10035	0.89
a-Si:H passivated	0.80	Si PM S10985-050C	0.79
a-Si:H_non-passivated	0.99	Si PM S10362-11-025U	0.77
CCD with indium tin oxide (ITO) gates with microlenses	0.83	Si PM S10362-11-050U	0.79
CCD with indium tin oxide (ITO) gates	0.75	Si PM S10362-11-100U	0.78
CCD with polygates	0.59	Flat panel PS-PMT H8500C-03	0.38
CCD no poly-gates LoD	0.82	Flat panel PS-PMT H8500D-03	0.30
CCD with traditional poly gates	0.87	Flat panel PS-PMT H10966A	0.29
CMOS (photogate array 0.5 μm)	0.76	Flat panel PS-PMT H8500C	0.37
CMOS RadEye HR	0.89	Bialkali photocathode	0.31
GaAs photocathode	0.97	Multialkali photocathode	0.58

scattered, *K* or *L*-fluorescence, and bremsstrahlung radiations interacting within the crystal. Thereafter the higher percentage of the heavier lutetium in LuAG and LSO result in higher EAE and almost identical values across the examined energy range. The presence of gadolinium in LGSO results in moderate energy absorption across X-ray energies.

4. Conclusion

In the present study the absolute luminescence efficiency and the spectral compatibility of LuAG:Ce crystals were investigated under conditions usually met in X-ray imaging conditions. Efficiency values were compared with previously published data for LGSO:Ce and LSO:Ce single crystals, of equal coating thickness. Peak absolute luminescence efficiency was obtained at 130 kVp for the 5 × 5 × 10 mm^3 LuAG:Ce crystal (31.86 E.U). The luminescence efficiency of the

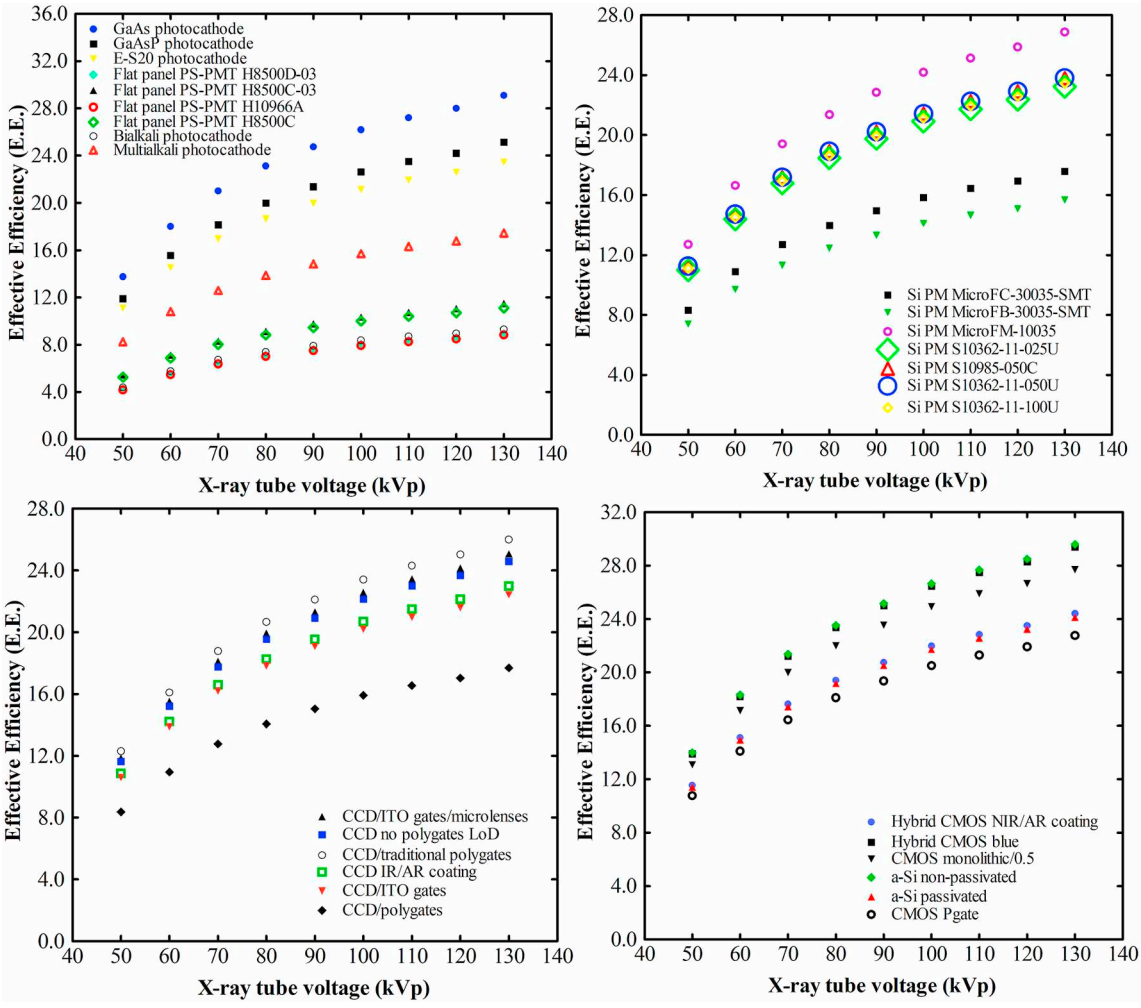

Fig. 3. Effective efficiency of the LuAG:Ce crystal combined with various light detectors.

Table 2
Energy absorption efficiency of a 10 mm thick LuAG:Ce crystal and comparison with LGSO:Ce and LSO:Ce single crystals.

X-ray tube voltage	X-ray energy absorption efficiency		
	$Lu_3Al_5O_{12}$:Ce	$(Lu50\%,Gd50\%)_2SiO_5$:Ce	Lu_2SiO_5:Ce
50	0.872	0.877	0.875
60	0.857	0.861	0.862
70	0.840	0.723	0.846
80	0,788	0.614	0.795
90	0.682	0.543	0.688
100	0.619	0.511	0.624
110	0.585	0.500	0.590
120	0.567	0.498	0.572
130	0.558	0.501	0.563

$10 \times 10 \times 10$ mm^3 LuAG:Ce crystal was found higher than both LGSO:Ce and LSO:Ce crystals, in the whole X-ray tube voltage range. The emission spectrum of LuAG:Ce showed an excellent match with the spectral sensitivities of photocathodes, charge-coupled devices, non-passivated amorphous hydrogenated silicon photodiodes (a-Si:H) and complementary metal-oxide semiconductors, employed in microelectronic radiation detectors. Considering the high luminescence efficiency values and the spectral compatibility with various photodetectors, LuAG:Ce could be potentially considered for use in medical imaging modalities, such as PET/CT scanners.

CRediT authorship contribution statement

C. Michail:Conceptualization, Writing - original draft.**K. Ninos**:Visualization.**N. Kalyvas**:Investigation, Writing - review & editing.**A. Bakas**:Resources.**G. Saatsakis**:Investigation.**G. Fountos**:Methodology, Validation.**I. Sianoudis**:Resources.**G. Panayiotakis**:Supervision.**I. Kandarakis**:Writing - review & editing.**I. Valais**:Conceptualization, Data curation.

Declaration of competing interest

The authors declare that they have no known competing financial interests or personal relationships that could have appeared to influence the work reported in this paper.

References

[1] M. Béranger, N. Vallet, M. Dorel, P. Huet, K. Cadoret, QALT study of scintillating material in digital flat panels for medical imaging, Microelectron. Reliab. 51 (2011) 1801–1805.
[2] M. Béranger, Use of a silicon drift detector for cathodoluminescence detection, Microelectron. Reliab. 55 (2015) 1569–1573.
[3] W. Chewpraditkul, L. Swiderski, M. Moszynski, T. Szczesniak, A. Syntfeld-Kazuch, C. Wanarak, P. Limsuwan, Scintillation properties of LuAG:Ce, YAG:Ce and LYSO:Ce crystals for gamma-ray detection, IEEE Trans. Nucl. Sci. 56 (2009) 3800–3805.
[4] C. Michail, G. Karpetas, N. Kalyvas, I. Valais, I. Kandarakis, K. Agavanakis, G. Panayiotakis, G. Fountos, Information capacity of positron emission tomography scanners, Crystals 8 (12) (2018) 459.
[5] J. Mares, M. Nikl, A. Beitlerova, P. Horodysky, K. Blazek, K. Bartos, C. D'Ambrosio, Scintillation properties of Ce^{3+}-and Pr^{3+}-doped LuAG, YAG and mixed $Lu_xY_{1-x}AG$ garnet crystals, IEEE Trans. Nucl. Sci. 59 (5) (2012) 2120–2125.
[6] J. Mares, A. Beitlerova, M. Nikl, A. Vedda, C. D'Ambrosio, K. Blazek, K. Nejezchleb, Time development of scintillating response in Ce- or Pr-doped crystals, Phys. Stat. Sol. C. 4 (3) (2007) 996–999.
[7] Z. Hu, X. Chen, H. Chen, Y. Shi, X. Liu, T. Xie, H. Kou, Y. Pan, E. Mihokova, M. Nikl, J. Li, Suppression of the slow scintillation component of Pr:$Lu_3Al_5O_{12}$ transparent ceramics by increasing Pr concentration, J. Lumin. 210 (2019) 14–20.
[8] M. Nikl, J. Pejchal, E. Mihokova, J. Mares, H. Ogino, A. Yoshikawa, T. Fukuda, A. Vedda, C. D'Ambrosio, Antisite defect-free $Lu_3(Ga_xAl_{1-x})_5O_{12}$:Pr$Lu_3(Ga_xAl_{1-x})_5O_{12}$:Pr scintillator, Appl. Phys. Lett. 88 (2006) 141916.
[9] K. Kamada, K. Tsutsumi, Y. Usuki, H. Ogino, T. Yanagida, A. Yoshikawa, Crystal growth and scintillation properties of 2-inch-diameter Pr:$Lu_3Al_5O_{12}$ (Pr:LuAG) single crystal, IEEE Trans. Nucl. Sci. 55 (3) (2008) 1488–1491.
[10] A. Yoshikawa, T. Yanagida, K. Kamada, Y. Yokota, J. Pejchal, Y. Usuki, S. Yamamoto, M. Miyake, K. Kumagai, A. Yamaji, K. Sasaki, T. dos Santos, M. Baba, M. Ito, M. Takeda, N. Ohuchi, M. Nikl, Positron emission mammography using Pr:LuAG scintillator — fusion of optical material study and systems engineering, Opt. Mater. 32 (2010) 1294–1297.
[11] M. Pan, C. Chen, M. Pan, Y. Shyr, Near infrared tomographic system based on high angular resolution mechanism – design, calibration, and performance, Measur 42 (3) (2009) 377–389.
[12] T. Yanagida, A. Yoshikawa, Y. Yokota, K. Kamada, Y. Usuki, S. Yamamoto, M. Miyake, M. Baba, K. Kumagai, K. Sasaki, M. Ito, N. Abe, Y. Fujimoto, S. Maeo, Y. Furuya, H. Tanaka, A. Fukabori, T. Rodrigues dos Santos, M. Takeda, N. Ohuchi, Development of Pr:LuAG scintillator array and assembly for positron emission mammography, IEEE Trans. Nucl. Sci. 57 (3) (2010) 1492–1495.
[13] G. Saatsakis, N. Kalyvas, C. Michail, K. Ninos, A. Bakas, C. Fountzoula, I. Sianoudis, G. Karpetas, G. Fountos, I. Kandarakis, I. Valais, G. Panayiotakis, Optical characteristics of ZnCuInS/ZnS (core/shell) nanocrystal flexible films under X-ray excitation, Crystals 9 (2019) 343.
[14] I. Seferis, C. Michail, J. Zeler, N. Kalyvas, I. Valais, G. Fountos, A. Bakas, I. Kandarakis, E. Zych, G.S. Panayiotakis, Detective quantum efficiency (DQE) of high X-ray absorption Lu_2O_3:Eu thin screens: the role of shape and size of nano- and micro-grains, Appl. Phys. A Mater. Sci. Process. 124 (2018) 604.
[15] G. Saatsakis, C. Michail, C. Fountzoula, N. Kalyvas, A. Bakas, K. Ninos, G. Fountos, I. Sianoudis, I. Kandarakis, G.S. Panayiotakis, I. Valais, Fabrication and luminescent properties of Zn-Cu-In-S/ZnS quantum dot films under UV excitation, Appl. Sci. 9 (2019) (2019) 2367.
[16] C. Michail, I. Valais, N. Martini, V. Koukou, N. Kalyvas, A. Bakas, I. Kandarakis, G. Fountos, Determination of the detective quantum efficiency (DQE) of CMOS/CsI imaging detectors following the novel IEC 62220-1-1:2015 international standard, Radiat. Meas. 94 (2016) 8–17.
[17] T. Kato, J. Kataoka, T. Nakamori, T. Miura, H. Matsuda, K. Sato, Y. Ishikawa, N. Kawabata, H. Ikeda, G. Sato, K. Kamada, Development of a large-area monolithic 4×4 MPPC array for a future PET scanner employing pixelized Ce:LYSO and Pr:LuAG crystals, Nucl. Instrum. Meth. Phys. Res. A. 638 (2011) 83–91.
[18] C. Hu, J. Li, F. Yang, B. Jiang, L. Zhang, R. Zhu, LuAG ceramic scintillators for future HEP experiments, Nucl. Instrum. Meth. Phys. Res. A (2019), https://doi.org/10.1016/j.nima.2018.12.038 in press.
[19] A. Kastengren, Thermal behavior of single-crystal scintillators for high-speed X-ray imaging, J. Synchrotron. Rad. 26 (2019) 205–214.
[20] S. Gundacker, R. Martinez Turtos, E. Auffray, M. Paganoni, P. Lecoq, High-frequency SiPM readout advances measured coincidence time resolution limits in TOF-PET, Phys. Med. Biol. 64 (2019) 055012.
[21] C. Michail, N. Kalyvas, A. Bakas, K. Ninos, I. Sianoudis, G. Fountos, I. Kandarakis, G. Panayiotakis, I. Valais, Absolute luminescence efficiency of europium-doped calcium fluoride (CaF_2:Eu) single crystals under X-ray excitation, Crystals 9 (5) (2019) 234.
[22] C. Van Eijk, Inorganic scintillators in medical imaging, Phys. Med. Biol. 47 (2002) R85–R106.
[23] C. Michail, G. Karpetas, G. Fountos, N. Kalyvas, I. Valais, C. Fountzoula, A. Zanglis, I. Kandarakis, G. Panayiotakis, A novel method for the optimization of positron emission tomography scanners imaging performance, Hell. J. Nucl. Med. 19 (3) (2016) 231–240.
[24] S. Witkiewicz-Lukaszek, V. Gorbenko, T. Zorenko, K. Paprocki, O. Sidletskiy, I. Gerasymov, J. Mares, R. Kucerkova, M. Nikl, Y. Zorenko, Novel all-solid-state composite scintillators based on the epitaxial structures of LuAG garnet doped with Pr, Sc, and Ce ions, IEEE Trans. Nucl. Sci. 65 (8) (2018) 2114–2119.
[25] S. Gundacker, F. Acerbi, E. Auffray, A. Ferri, A. Gola, M. Nemallapudi, G. Paternoster, C. Piemonteban, P. Lecoq, State of the art timing in TOF-PET detectors with LuAG, GAGG and L(Y)SO scintillators of various sizes coupled to FBK-SiPMs, J. Instrum. 11 (2016) P08008.
[26] W. Chewpraditkul, L. Swiderski, M. Moszynski, T. Szczesniak, A. Syntfeld-Kazuch, C. Wanarak, P. Limsuwan, Scintillation properties of LuAG:Ce, YAG:Ce and LYSO:Ce crystals for gamma-ray detection, IEEE Trans. Nucl. Sci. 56 (2009) 3800–3805.
[27] W. Chewpraditkul, M. Moszynski, Scintillation properties of $Lu_3Al_5O_{12}$, Lu_2SiO_5 and $LaBr_3$ crystals activated with cerium, Phys. Procedia 22 (2011) 218–226.
[28] M. Nikl, A. Yoshikawa, Recent R&D trends in inorganic single-crystal scintillator materials for radiation detection, Adv. Optical Mater. 3 (2015) 463–481.
[29] M. Lucchini, O. Buganov, E. Auffray, P. Bohacek, M. Korjik, D. Kozlov, S. Nargelas, M. Nikl, S. Tikhomirov, G. Tamulaitis, A. Vaitkevicius, K. Kamada, A. Yoshikawa, Measurement of non-equilibrium carriers dynamics in Ce-doped YAG, LuAG and GAGG crystals with and without Mg-codoping, J. Lumin. 194 (2018) 1–7.
[30] K. Sreebunpeng, W. Chewpraditkul, M. Nikl, Light yield and light loss coefficient of LuAG:Ce and LuAG:Pr under excitation with α- and γ-rays, J. Cryst. Growth 468 (2017) 373–375.
[31] M. Lucchini, K. Pauwels, K. Blazek, S. Ochesanu, E. Auffray, Radiation tolerance of LuAG:Ce and YAG:Ce crystals under high levels of gamma- and proton-irradiation, IEEE Trans. Nucl. Sci. 63 (2016) 586–590.
[32] H. Ogino, A. Yoshikawa, M. Nikl, K. Kamada, T. Fukuda, Scintillation characteristics of Pr-doped $Lu_3Al_5O_{12}$ single crystals, J. Cryst. Growth 292 (2006) 239–242.
[33] H. Li, X. Liu, L. Huang, Fabrication of transparent cerium-doped lutetium aluminum garnet (LuAG:Ce) ceramics by a solid-state reaction method, J. Am. Ceram. Soc. 88 (2005) 3226–3228.
[34] M. Nikl, V. Babin, J.A. Mares, K. Kamada, S. Kurosawa, A. Yoshikawa, J. Tous, J. Houzvicka, K. Blazek, The role of cerium variable charge state in the luminescence and scintillation mechanism in complex oxide scintillators: the effect of air annealing, J. Lumin. 169 (B) (2016) 539–543.

[35] S. Liu, X. Feng, J. Mares, V. Babin, M. Nikl, A. Beitlerova, Y. Shi, Y. Zeng, Y. Pan, C. D'Ambrosio, Y. Huang, Optical, luminescence and scintillation characteristics of non-stoichiometric LuAG:Ce ceramics, J. Lumin. 169 (2016) 72–77.
[36] M. Nikl, A. Yoshikawa, K. Kamada, K. Nejezchleb, C. Stanek, J. Mares, K. Blazek, Development of LuAG-based scintillator crystals—a review, Prog. Cryst. Growth Charact. Mater. 59 (2013) 47–72.
[37] J. Ogieglo, A. Zych, T. Jüstel, A. Meijerink, C. Ronda, Luminescence and energy transfer in $Lu_3Al_5O_{12}$ scintillators co-doped with Ce^{3+} and Pr^{3+}, Opt. Mater. 35 (2013) 322–331.
[38] L. Swiderski, M. Moszynski, A. Nassalski, A. Syntfeld-Kazuch, T. Szczesniak, K. Kamada, K. Tsutsumi, Y. Usuki, T. Yanagida, A. Yoshikawa, W. Chewpraditkul, M. Pomorski, Scintillation properties of praseodymium doped LuAG scintillator compared to cerium doped LuAG, LSO and $LaBr_3$, IEEE Trans. Nucl. Sci. 56 (4) (2009) 2499–2505.
[39] M. Kobayashi, S. Aogaki, F. Takeutchi, Y. Tamagawa, Y. Usuki, Performance of thin long scintillator strips of GSO:Ce, LGSO:Ce and LuAG:Pr for low energy γ-rays, Nucl. Instrum. Meth. Phys. Res. A 693 (2012) 226–235.
[40] Y. Kuwano, K. Suda, N. Ishizawa, T. Yamada, Crystal growth and properties of $(Lu, Y)_3Al_5O_{12}$, J. Cryst. Growth 260 (1–2) (2004) 159–165.
[41] K. Brylew, W. Drozdowski, M. Witkowski, K. Kamada, T. Yanagida, A. Yoshikawa, Effect of thermal annealing in air on scintillation properties of LuAG and LuAG:Pr, Cent. Eur. J. Phys. 11 (1) (2013) 138–142.
[42] M. Witkowski, D. Zhou, W. Drozdowski, J. Xu, Scintillation properties and effect of thermal annealing in $Lu_3Al_5O_{12}$:Ce and $Lu_3Al_5O_{12}$:Pr ceramics, Opt. Mater. 85 (2018) 230–237.
[43] S. Liu, J. Mares, V. Babin, C. Hu, H. Kou, C. D'Ambrosio, J. Li, Y. Pan, M. Nikl, Composition and properties tailoring in Mg^{2+} codoped non-stoichiometric LuAG:Ce, Mg scintillation ceramics, J. Eur. Ceram. Soc. 37 (2017) 1689–1694.
[44] Y. Zhang, Y. Zhang, Y. Zhang, H. Gong, Synthesis and characteristics of fine crystalline LuAG:Ce phosphors by microwave-induced solution combustion method, J. Lumin. 181 (2017) 360–366.
[45] L. Pan, B. Jiang, J. Fan, Q. Yang, C. Zhou, P. Zhang, X. Mao, L. Zhang, Preparation of LuAG powders with single phase and good dispersion for transparent ceramics using co-precipitation method, Materials 8 (2015) 5363–5375.
[46] Y. Zorenko, P. Douissard, T. Martin, F. Riva, V. Gorbenko, T. Zorenko, K. Paprocki, A. Iskalieva, S. Witkiewicz, A. Fedorov, P. Bilski, A. Twardak, Scintillating screens based on the LPE grown $Tb_3Al_5O_{12}$:Ce single crystalline films, Opt. Mater. 65 (2017) 73–81.
[47] P. Prusa, M. Kucera, J. Mares, M. Nikl, K. Nitsch, M. Hanus, Z. Onderisinova, T. Cechak, Scintillation properties of Sc-, Pr-, and Ce-doped LuAG epitaxial garnet films, J. Cryst. Growth 218 (2011) 545–548.
[48] Y. Zorenko, V. Gorbenko, E. Mihokova, M. Nikl, K. Nejezchleb, A. Vedda, V. Kolobanov, D. Spassky, Single crystalline film scintillators based on Ce- and Pr-doped aluminium garnets, Radiat. Measur. 42 (2007) 521–527.
[49] M. Derdzyan, K. Ovanesyan, A. Petrosyan, A. Belsky, C. Dujardin, E. Auffray, P. Lecoq, M. Lucchini, K. Pauwels, Radiation hardness of LuAG:Ce and LuAG:Pr scintillator crystals, J. Cryst. Growth 361 (2012) 212–216.
[50] K. Ivanovskikh, J. Ogieglo, A. Zych, C. Ronda, A. Meijerink, Luminescence temperature quenching for Ce^{3+} and Pr^{3+} d-f emission in YAG and LuAG, ECS J. Solid State Sci. Technol. 2 (2) (2013) R3148–R3152.
[51] D. Nikolopoulos, I. Valais, C. Michail, A. Bakas, C. Fountzoula, D. Cantzos, D. Bhattacharyya, I. Sianoudis, G. Fountos, P. Yannakopoulos, G. Panayiotakis, I. Kandarakis, Radioluminescence properties of the CdSe/ZnS quantum dot nanocrystals with analysis of long-memory trends, Radiat. Meas. 92 (2016) 19–31.
[52] C. Michail, I. Valais, G. Fountos, A. Bakas, C. Fountzoula, N. Kalyvas, A. Karabotsos, I. Sianoudis, I. Kandarakis, Luminescence efficiency of calcium tungstate ($CaWO_4$) under X-ray radiation: comparison with Gd_2O_2S:Tb, Measur 120 (2018) 213–220.
[53] G. Saatsakis, C. Michail, C. Fountzoula, N. Kalyvas, K. Ninos, A. Bakas, I. Sianoudis, I. Kandarakis, G. Fountos, G. Panayiotakis, I. Valais, Luminescence efficiency of Zn-Cu-In-S/ZnS quantum dot films, IEEE Xplore (2019) 1–4.
[54] Hamamatsu Photonics, MPPC (multi-pixel photon counters), http://www.hamamatsu.com/us/en/product/category/3100/4004/4113/index.html#.
[55] SensL, Silicon photomultipliers, http://sensl.com/products/silicon-photomultipliers/.
[56] J. Rowlands, J. Yorkston, Flat panel detectors for digital radiography, in: J. Beutel, H. Kundel, R. Van Metter (Eds.), Handbook of Medical Imaging: Physics and Psychophysics, SPIE, Bellingham, 2000, pp. 223–328.
[57] P. Magnan, Detection of visible photons in CCD and CMOS: a comparative view, Nucl. Instrum. Meth. Phys. Res. A. 504 (2003) 199–212.
[58] J. Hubbell, S. Seltzer, Tables of X-ray Mass Attenuation Coefficients and Mass Energy Absorption Coefficients 1 to 20 MeV for Elements Z = 1 to 92 and 48 Additional Substances of Dosimetric Interest. US Department of Commerce, NISTIR 5632, (1995).
[59] D. Cavouras, I. Kandarakis, A. Bakas, D. Triantis, C. Nomicos, G. Panayiotakis, An experimental method to determine the effective luminescence efficiency of scintillator-photodetector combinations used in X-ray medical imaging systems, Br. J. Radiol. 71 (1998) 766–772.
[60] R. Evans, The Atomic Nucleus, McGraw-Hill, New York, 1955.
[61] J. Seibert, J. Boone, X-ray imaging physics for nuclear medicine technologists. Part 2: X-ray interactions and image formation, J. Nucl. Med. Technol. 33 (2005) 3–18.
[62] E. Storm, H. Israel, Report LA-3753, Los Alamos Scientific Laboratory, University of California, CA, 1967.
[63] A. Petrosyan, K. Ovanesyan, M. Derdzyan, I. Ghambaryan, G. Patton, F. Moretti, E. Auffray, P. Lecoq, M. Lucchini, K. Pauwels, C. Dujardin, A study of radiation effects on LuAG:Ce(Pr) co-activated with Ca, J. Cryst. Growth 430 (2015) 46–51.
[64] C. Dujardin, C. Mancini, D. Amans, G. Ledoux, D. Abler, E. Auffray, P. Lecoq, D. Perrodin, A. Petrosyan, K.L. Ovanesyan, LuAG:Ce fibers for high energy calorimetry, J. Appl. Phys. 108 (2010) 13510.
[65] O. Sidletskiy, P. Arhipov, S. Tkachenko, O. Zelenskaya, S. Vasyukov, F. Moretti, C. Dujardin, Drastic scintillation yield enhancement of YAG:Ce with carbon doping, Phys. Status. Solidi. A 215 (2018) 1800122.